

SELECTION TRIGGER FOR RARE QUARK-GLUON PLASMA FORMATION EVENTS

G.H. Arakelyan¹, C. Merino², and Yu.M. Shabelski³

¹A.Alikhanyan National Scientific Laboratory
Yerevan Physics Institute
Yerevan, 0036, Armenia
E-mail: argev@mail.yerphi.am

²Departamento de Física de Partículas, Facultade de Física
and Instituto Galego de Física de Altas Enerxías (IGFAE)
Universidade de Santiago de Compostela
Santiago de Compostela 15782
Galiza, Spain
E-mail: merino@fpaxp1.usc.es

³Petersburg Nuclear Physics Institute
NCR Kurchatov Institute
Gatchina, St.Petersburg 188350, Russia
E-mail: shabelsk@thd.pnpi.spb.ru

A b s t r a c t

We consider the experimental ratios of multistrange to strange antibaryon production and compare them to the standard Quark-Gluon String Model predictions. The significant differences between the experimental $\Xi^+/\bar{\Lambda}$ and, especially, $\bar{\Omega}^+/\bar{\Lambda}$ values and model predictions can be interpreted as the signal of the existence of an additional source of multistrange antibaryon production. The possible connection of this additional source with Quark-Gluon Plasma (QGP) formation can turn the $\bar{\Omega}^+$ production into a good QGP signature.

PACS. 25.75.Dw Particle and resonance production

1 Introduction

The Quark-Gluon String Model (QGSM) [1, 2] is based on the Dual Topological Unitarization (DTU), Regge phenomenology and nonperturbative notions of QCD. This model is successfully used for the description of multiparticle production processes in hadron-hadron [2, 3, 4, 5], hadron-nucleus [6, 7], and nucleus-nucleus [8, 9, 10] collisions. In particular, the rapidity dependence of the inclusive densities of different secondaries (π^\pm , K^\pm , p , and \bar{p}) [10] produced in $Pb + Pb$ collisions, and of the net baryon ($p - \bar{p}$ and $\Lambda - \bar{\Lambda}$) [11] on nuclear targets at CERN SpS energies, have been reasonably described in the framework of QGSM.

In QGSM high energy interactions are considered as proceeding via the exchange of one or several Pomerons. The cut of the elastic scattering amplitude determines the particle production processes which occur via production and subsequent decay of the quark-gluon strings.

In the case of interaction with a nuclear target, the Multiple Scattering Theory (Gribov-Glauber Theory) is used. For nucleus-nucleus collisions, the Multiple Scattering Theory also allows to consider this interactions as the superposition of separate nucleon-nucleon interactions. However, in this case the analytical summation of all the diagrams is impossible [12]. The significant classes of diagrams can be summed up analytically in the so-called rigid target approximation [13], which will be used in the present paper.

At very high energies, the contribution of enhancement Reggeon diagrams (percolation effects) becomes important, what leads to a new phenomenological effect, the suppression of the inclusive density of secondaries [14] into the average central (midrapidity) region. This corresponds to a significant fusion of the produced quark-gluon strings. In the energy limit when the probability of this fusions is very large, one should expect the appearance of a new state of matter, the Quark-Gluon Plasma (QGP). However, the process of QGP production can already occur with small probability at a not so high energy.

In this paper we present the ratios of multistrange to strange antihyperon production in the collision of projectile A (nucleon or nucleus) with a nuclear target B. Let us define:

$$R(\Xi^+/\bar{\Lambda}) = \frac{dn}{dy}(A + B \rightarrow \Xi^+ + X) / \frac{dn}{dy}(A + B \rightarrow \bar{\Lambda} + X) , \quad (1)$$

$$R(\bar{\Omega}^+/\bar{\Lambda}) = \frac{dn}{dy}(A + B \rightarrow \bar{\Omega}^+ + X) / \frac{dn}{dy}(A + B \rightarrow \bar{\Lambda} + X) . \quad (2)$$

The produced antihyperons, Ξ^+ and $\bar{\Omega}^+$, contain valence antiquarks newly produced

during the collision. The ratios in Eqs. (1) and (2) are reasonably described by QGSM in the cases when a not very large number of incident nucleons participate in the collision (nucleon-nucleus or peripheral nucleus-nucleus collisions).

The number of quark-gluon strings (cut pomerons) in nucleus-nucleus collisions increases with centrality. If the secondaries are produced independently in every quark-gluon string, the ratio of yields of different particles should not depend on centrality. However, experimentally the enhancement of the yield of Ξ^+ is stronger than that of $\bar{\Lambda}$, and for $\Omega^- + \bar{\Omega}^+$ the enhancement is also stronger than for Ξ^+ (e.g. see [15]). This means that an additional source of multistrange hyperons appears from collective interactions of several strings, and this additional source can be considered as a QGP state effect.

In the present paper we consider the central Pb+Pb collisions. The experimental ratios of Eqs. (1) and (2), as functions of centralities, are in total disagreement with the standard QGSM predictions, where it is assumed that each secondary particle is produced by the independent fragmentation of every quark-gluon string. We can now assume that some new contribution to the multistrange antihyperon formation appears in this case of central Pb+Pb collisions (see Sections 3 and 4). This new contribution, that is not accounted for in the standard QGSM scheme, could be seen as a signature of QGP production in some small volume of the interaction region.

2 Production of Secondaries in the QGSM

The QGSM [1, 2] allows one to make quantitative predictions of different features of multiparticle production, in particular, the inclusive densities of different secondaries both in the central and in the beam fragmentation regions. In QGSM, high energy hadron-nucleon collisions are implemented through the exchange of one or several Pomerons, all elastic and inelastic processes resulting from cutting through or between Pomerons [16].

Each Pomeron corresponds to a cylindrical diagram, and thus, when cutting one Pomeron, two showers of secondaries are produced (see Fig. 1a,1b).

The inclusive spectrum of a secondary hadron h is then determined by the convolution of the diquark, valence quark, and sea quark distributions $u(x, n)$ (where every distribution $u_i(x, n)$ is normalized to unity) in the incident particles, with the fragmentation functions $G^h(z)$ of quarks and diquarks into the secondary hadron h . These distributions, as well as the fragmentation functions, are constructed using the Reggeon counting rules [17].

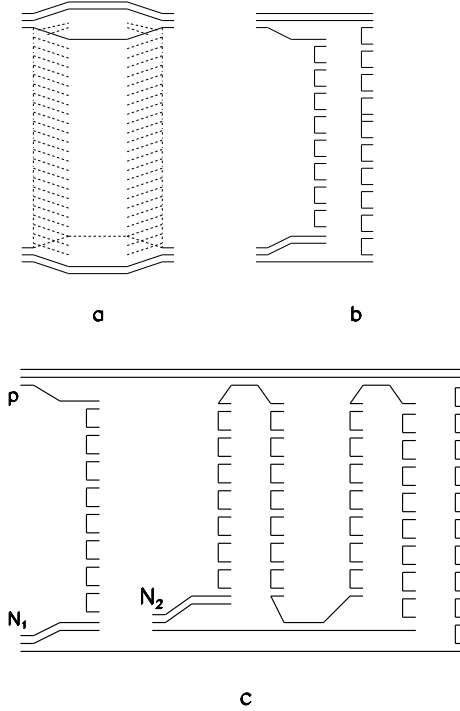


Figure 1: (a) Cylindrical diagram representing the Pomeron exchange within the DTU classification. Quarks are shown by solid lines; (b) Cut of the cylindrical diagram corresponding to the single-Pomeron exchange contribution in inelastic pp scattering; (c) Diagram corresponding to the inelastic interaction of an incident proton with two target nucleons N_1 and N_2 in a pA collision.

In particular, in the case of $n > 1$, i.e. in the case of multipomeron exchange, the distributions of valence quarks and diquarks are softened due to the appearance of a new contribution from sea quarks-antiquarks.

The details of the model are presented in [1, 2, 3, 18]. The average number of exchanged Pomerons $\langle n \rangle_{pp}$ slowly increase with the energy. The values of the Pomeron parameters have been taken from [3].

For a nucleon target, the inclusive rapidity, y , or Feynman- x , x_F , spectrum of a secondary hadron h has the form [1]:

$$\frac{dn}{dy} = \frac{x_E}{\sigma_{inel}} \cdot \frac{d\sigma}{dx_F} = \sum_{n=1}^{\infty} w_n \cdot \phi_n^h(x) + w_D \cdot \phi_D^h(x) , \quad (3)$$

where the functions $\phi_n^h(x)$ determine the contribution of diagrams with n cut Pomerons, w_n is the relative weight of this diagram, and the term $w_D \cdot \phi_D^h(x)$ accounts for the contribution of diffraction dissociation processes.

For pp collisions

$$\phi_n^h(x) = f_{qq}^h(x_+, n) \cdot f_q^h(x_-, n) + f_q^h(x_+, n) \cdot f_{qq}^h(x_-, n) + 2(n-1)f_s^h(x_+, n) \cdot f_s^h(x_-, n) , \quad (4)$$

$$x_{\pm} = \frac{1}{2}[\sqrt{4m_T^2/s + x^2} \pm x] , \quad (5)$$

where f_{qq} , f_q , and f_s correspond to the contributions of diquarks, valence quarks, and sea quarks, respectively.

These contributions are determined by the convolution of the diquark and quark distributions with the fragmentation functions, e.g.,

$$f_q^h(x_+, n) = \int_{x_+}^1 u_q(x_1, n) \cdot G_q^h(x_+/x_1) dx_1 . \quad (6)$$

In the calculation of the inclusive spectra of secondaries produced in pA collisions we should consider the possibility of one or several Pomeron cuts in each of the ν blobs of proton-nucleon inelastic interactions. For example, in Fig. 1c it is shown one of the diagrams contributing to the inelastic interaction of a beam proton with two target nucleons. In the blob of the proton-nucleon1 interaction one Pomeron is cut, and in the blob of the proton-nucleon2 interaction two Pomerons are cut. The details can be found in [6].

It is essential to take into account all digrams with every possible Pomeron configuration and its permutations. The diquark and quark distributions and the fragmentation functions here are the same as in the case of pN interaction.

The total number of exchanged Pomerons becomes as large as

$$\langle n \rangle_{pA} \sim \langle \nu \rangle_{pA} \cdot \langle n \rangle_{pN} , \quad (7)$$

where $\langle \nu \rangle_{pA}$ is the average number of inelastic collisions inside the nucleus (about 4 for heavy nuclei at SpS energies).

The process shown in Fig. 1c satisfies [19, 20, 21, 22] the condition that the absorptive parts of the hadron-nucleus amplitude are determined by the combination of the absorptive parts of the hadron-nucleon amplitudes.

In the case of a nucleus-nucleus collision, we use in the fragmentation region of the projectile the approach in refs. [8, 9, 10], where the beam of independent nucleons of the projectile interacts with the target nucleus, what corresponds to the rigid target approximation [13] of Glauber Theory. Correspondingly, in the target fragmentation

region the beam of independent target nucleons interacts with the projectile nucleus. The results obtained on the two fragmentation regions coincide in the central region. The corrections for energy conservation play here a very important role when the initial energy is not very high. This approach was used in [10] for the successful description of π^\pm , K^\pm , p , and \bar{p} produced in Pb+Pb collisions at 158 GeV per nucleon.

3 Inclusive Spectra with String Fusion and Percolation Effects

The QGSM gives a reasonable description [5, 6, 10] of the inclusive spectra on nuclear targets at energies $\sqrt{s_{NN}} = 14\text{--}30$ GeV. At RHIC energies the situation drastically changes. The spectra of secondaries produced in pp collisions are described by QGSM rather well [5], but the RHIC experimental data for Au+Au collisions [23, 24] give clear evidence of the suppression effects which reduce the midrapidity inclusive density by about a factor two when compared to the predictions based on the superposition picture [25, 26, 27]. This reduction can be explained by the inelastic screening corrections connected to multipomeron interactions [14] (see Fig. 2).

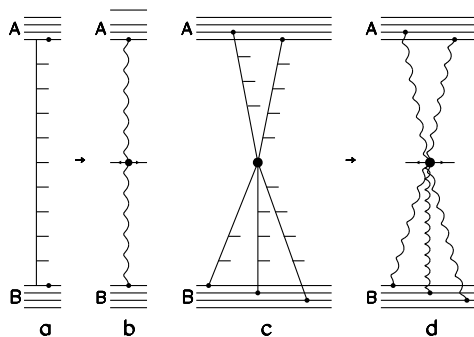


Figure 2: (a) Multipomeron ladder diagram; (b) Inclusive cross section to which diagram (a) corresponds; (c) Diagram with fusion of several ladders; (d) Inclusive cross section to which diagram (c) corresponds.

At fixed target energies, $\sqrt{s_{NN}} \leq 30$ GeV, the nucleus-nucleus interaction can be described as the sum of one-Pomeron and of multipomeron eikonal exchanges. The inelastic processes are then determined by the production of one (Fig. 2a), or several multipomeron ladders, and the corresponding inclusive cross sections are described by the diagram of Fig. 2b.

In accordance with the Parton Model [28, 29], the fusion of multiperipheral ladders shown in Fig. 2c becomes essential when the energy increases, what should reduce the inclusive density of secondaries. Such processes correspond to the enhancement Reggeon diagrams shown in Fig. 2d, and with more complicated ones. All these diagrams are proportional to the squared longitudinal form factors of both colliding nuclei [14]. Following the estimations presented in reference [14], the RHIC energies are just in the order of magnitude needed to observe this effect.

Unfortunately, all estimations are model dependent, since the numerical weight of the contribution of the multipomeron diagrams remains rather unclear due to the many unknown vertices in these diagrams. However, the number of unknown parameters can be reduced in some models, and, for example, in reference [14] the Schwimmer model [30] was used for the numerical calculations.

Another possibility to estimate the contribution of the diagrams with Pomeron interaction comes [31, 32, 33, 34, 35] from Percolation Theory. The percolation approach and its previous version, the String Fusion Model [36, 37, 38], predicted the multiplicity suppression seen at RHIC energies long before any RHIC data were taken.

New calculations of inclusive densities and multiplicities in percolation theory, both in pp [39, 40] and in heavy ion collisions [40, 41], are in a good agreement with the experimental data for a wide energy region.

In the percolation approach one assumes that if two or several Pomerons overlap in transverse space, they fuse in only one Pomeron. When all quark-gluon strings (cut Pomerons) are overlapping, the inclusive density saturates, reaching its maximal value at a given impact parameter.

This approach has only one free parameter, η [31, 32, 33, 34, 35]:

$$\eta = N_s \cdot \frac{r_s^2}{R^2} \cdot \langle r(y) \rangle , \quad (8)$$

with N_s the number of produced strings, r_s the string transverse radius, and R the radius of the overlapping area. The factor $\langle r(y) \rangle$ accounts for the fact that the parton density near the ends of the string is smaller than in the central region, where we fix $r(0) = 1$. At large rapidities, we have N_s strings with different parton densities, $r_i(y)$, and

$$N_s \cdot \langle r(y) \rangle = \sum_{i=1}^{N_s} r_i(y) . \quad (9)$$

As a result, the bare inclusive density $dn/dy|_{bare}$ gets reduced, and we obtain:

$$dn/dy = F(\eta) \cdot dn/dy|_{bare} , \quad (10)$$

with [42]

$$F(\eta) = \sqrt{\frac{1 - e^{-\eta}}{\eta}}. \quad (11)$$

The number of quark-gluon strings (cut pomerons) increases with the centrality of the nucleus-nucleus collisions. If the secondaries are independently produced in every quark-gluon string, then the ratio of yields of different particles should not depend on the centrality of the collision. At not very high energies, as quark-gluon strings are usually not overlapped (see Fig. 3a), the parameter η is rather smaller. At very high energies, on the contrary, the value of η is large, and in every heavy ion collision quark-gluon strings can be overlapped, as it is shown in Fig. 3b.

However, experimentally, even at not very high energies (e.g. see [15]), the yield of Ξ^+ is more strongly enhanced than that of $\bar{\Lambda}$, and also the yield of $\Omega^- + \bar{\Omega}^+$ shows a stronger enhancement than the yield of Ξ^+ . This means that one additional source of multistrange hyperons must be at work from collective interactions of several strings.

At intermediate energies, we can think of rare situations when a few strings overlap in a small volume (see Fig. 3c). This can be possibly considered as a QGP state effect. This can occur when the density of produced quark-gluon strings is several times larger than its average value.

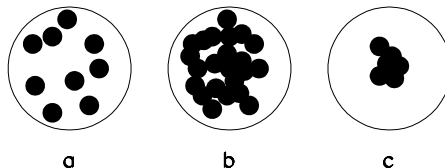


Figure 3: (a) Average heavy ion collisions at intermediate energies; (b) Average heavy ion collisions at very high energies; (c) Rare configuration when several strings overlap in a small volume. Quark-gluon strings are shown by black points.

Contrary to what happens in the case shown in Fig. 3a, for the configurations in Figs. 3b and 3c we can assume that the quark-gluon plasma has been produced. In the next section we will show that these rare configurations can possibly give a large contribution in the cases of Ξ^+ and, especially $\bar{\Omega}^+$, production.

When we consider central Pb+Pb collisions, we see that the experimental data on the ratios in Eqs. (1) and (2) are in disagreement with the standard QGSM predictions described in Section 2. The experimental ratios show very strong energy dependences as a function of centrality in the CERN SpS-RHIC energy interval. To account for

this effect, we can assume that some new contribution for multistrange antihyperon formation appears in this case. For example, the three strange antiquarks needed for the formation of $\bar{\Omega}^+$ could be taken at some energies out of three different quark-gluon strings, and not from the fragmentation of the same string. This could be possible if the multiplicity of newly produced strange-antistrange pairs would decrease with the number of pairs faster than, say, a Poissonian distribution. This new contribution is not included in the standard QGSM scheme, and it can be identified as a QGP formation signature.

Probably, when the energy increases the distribution of the number of strange-antistrange pairs corresponding to this new contribution decreases not so fast, and so the contribution from one quark-gluon string will dominate over the collective contributions. However, this effect appears to be very model dependent, so we will not consider its details in this paper.

In order to account for the percolation effects in the QGSM, it is technically more simple [43] to consider in the central region the maximal number of Pomerons n_{max} emitted by one nucleon that can be cut. These cut Pomerons lead then to the different final states, and the contributions of all diagrams with $n \leq n_{max}$ are accounted for as at lower energies. Larger number of Pomerons $n > n_{max}$ can also be emitted obeying the unitarity constraint, but due to fusion in the final state (at the quark-gluon string stage), the cut of $n > n_{max}$ Pomerons results in the same final state as the cut of n_{max} Pomerons.

The QGSM fragmentation formalism allows one to calculate the integrated over p_T spectra of different secondaries as function of the rapidity. The number of strings that can be used for the secondary production should increase with the initial energy, as it was shown in [44].

The contribution coming from the coherent interaction of two nuclear clusters [45] has been estimated following [11] to be not larger than (20-30)%.

4 Theoretical Results and Selection Trigger for Quark-Gluon Plasma Formation Events

4.1 NA49 Collaboration Data

The NA49 Collaboration obtained experimental data [46, 47] for yields of $\bar{\Lambda}$ and $\bar{\Xi}^+$ hyperons in midrapidity region ($|y| < 0.4$ for $\bar{\Lambda}$, and $|y| < 0.5$ for $\bar{\Xi}^+$) in central C+C,

Si+Si, and Pb+Pb collisions (5% centrality for $\bar{\Lambda}$, and 10% centrality for Ξ^+) at 158 GeV per nucleon. These results are presented in Table 1, together with the QGSM results calculated for the same rapidities and centralities.

We see a reasonable agreement for secondary $\bar{\Lambda}$, but the calculated yields of Ξ^+ are significantly smaller than those measured by the NA49 Collaboration. This disagreement can have very important implications that we will discuss in more detail in the next subsection.

Collision	QGSM	NA49 Collaboration
C+C $\rightarrow \bar{\Lambda}$	0.064	$0.064 \pm 0.003 \pm 0.010$
Si+Si $\rightarrow \bar{\Lambda}$	0.17	$0.16 \pm 0.007 \pm 0.038$
Pb+Pb $\rightarrow \bar{\Lambda}$	2.05	$1.4 \pm 0.3 \pm 0.2$
Pb+Pb $\rightarrow \Xi^+$	0.16	$0.31 \pm 0.03 \pm 0.03$

Table 1: Experimental data [46, 47] by the NA49 Collaboration for $\bar{\Lambda}$ and Ξ^+ production in central (5% centrality) C+C, Si+Si, and Pb+Pb collisions at 158 GeV per nucleon, and the corresponding QGSM results.

4.2 NA57 Collaboration Data

The NA57 Collaboration obtained the experimental data [48] for strange and multi-strange hyperon $\bar{\Lambda}$, Ξ^+ , and $\bar{\Omega}^+$ yields in the midrapidity region $|y| < 0.5$ in minimum bias p +Be and p +Pb reactions, and in central (5% centrality) Pb+Pb collisions, at 158 GeV per nucleon.

These data are presented in Table 2, together with the corresponding QGSM calculations.

Unfortunately, the data obtained by NA49 and NA57 Collaborations are not compatible, probably due to different experimental event selection. As one can see in Tables 1 and 2, the values of dn/dy for the different hyperons obtained by one collaboration are far outside the error bars of the values obtained at the same centrality by the other collaboration.

Collision	QGSM	NA57 Collaboration
$p+\text{Be} \rightarrow \bar{\Lambda}$	0.010	$0.011 \pm 0.0002 \pm 0.0001$
$p+\text{Be} \rightarrow \bar{\Xi}^+$	0.00081	$0.00077 \pm 0.0001 \pm 0.0001$
$p+\text{Be} \rightarrow \bar{\Omega}^+$	0,000042	$0,00074 \pm 0.0002 \pm 0.001$
$p+\text{Pb} \rightarrow \bar{\Lambda}$	0.019	$0.015 \pm 0.001 \pm 0.002$
$p+\text{Pb} \rightarrow \bar{\Xi}^+$	0.0015	$0.0012 \pm 0.001 \pm 0.001$
$p+\text{Pb} \rightarrow \bar{\Omega}^+$	0,000076	$0,0095 \pm 0.003 \pm 0.001$
$\text{Pb}+\text{Pb} \rightarrow \bar{\Lambda}$	2.05	$2.44 \pm 0.14 \pm 0.24$
$\text{Pb}+\text{Pb} \rightarrow \bar{\Xi}^+$	0.16	$0.51 \pm 0.04 \pm 0.05$
$\text{Pb}+\text{Pb} \rightarrow \bar{\Omega}^+$	0,006668	$0,16 \pm 0.04 \pm 0.02$

Table 2: Experimental data [48] obtained by the NA57 Collaboration for $\bar{\Lambda}$, $\bar{\Xi}^+$, and $\bar{\Omega}^+$ production in $p+\text{Be}$, $p+\text{Pb}$, and in central (5% centrality) $\text{Pb}+\text{Pb}$ collisions at 158 GeV per nucleon, and the corresponding QGSM results.

Here again one can see that the calculated yields of $\bar{\Lambda}$ are in agreement with the experimental data on the level of 20-30% accuracy. Inclusive densities of $\bar{\Xi}^+$ hyperons are reasonably reproduced for the cases of $p+\text{Be}$ and $p+\text{Pb}$ collisions, but are several times underestimated in the case of central $\text{Pb}+\text{Pb}$ interactions. For $\bar{\Omega}^+$ production in central $\text{Pb}+\text{Pb}$ collisions, the disagreement is larger than one order of magnitude. The reason to discuss the production of antihyperons in these processes is that since a large baryon charge already exists in the initial state, some hyperons can be produced via the final state interaction of any baryon with a strange meson, but, on the contrary, the production of multistrange antihyperon production would be a signal of the production of several strange antiquarks in some small space-time volume.

These effects are more evidently seen in Fig. 4, where the experimental ratios of $\bar{\Omega}^+/\bar{\Lambda}$ and $\bar{\Xi}^+/\bar{\Lambda}$ as functions of the number of participating nucleons, N_w , together with the corresponding QGSM results, shown by solid curves. The first two left points in every panel correspond to $p+\text{Be}$ and $p+\text{Pb}$ collisions, and the other points correspond to $\text{Pb}+\text{Pb}$ interactions with different centralities.

We consider the disagreement of the QGSM results with the experimental values as a signal of the quantitatively large new contribution of $\bar{\Omega}^+$ and $\bar{\Xi}^+$ production to the inclusive cross section. This new contribution could appear when strange antiquarks are taken from different Pomerons (quark-gluon strings), in some collective interaction (see Fig. 3c) that can be seen as at the origin of Quark-Gluon Plasma formation.

Thus, the selection of events with $\bar{\Xi}^+$, and especially with $\bar{\Omega}^+$ production, would allow the definition of a sample enriched by Quark-Gluon Plasma formation events,

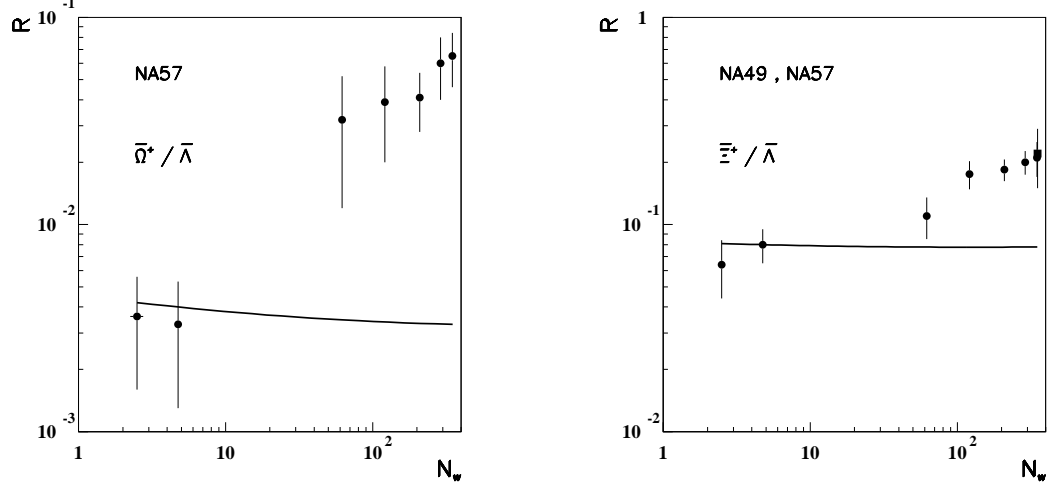


Figure 4: Ratios of $\bar{\Omega}^+$ to $\bar{\Lambda}$ (left panel), and of $\bar{\Xi}^+$ to $\bar{\Lambda}$ (right panel) as functions of the number of wounded nucleons, N_w . The experimental data for p+Be, p+Pb, and for Pb+Pb with different centralities measured by the NA57 Collaboration (points) and by the NA49 Collaboration (squares) are presented, together with the corresponding QGSM results, shown by solid curves.

and such a sample could be compared to a sample of events where only $\bar{\Lambda}$ hyperons are produced, to unravel QGP definite features.

4.3 STAR Collaboration Data

Hyperon production at higher energies in midrapidity region was measured at RHIC. The data [49] obtained by the STAR Collaboration for Au+Au collisions at $\sqrt{s_{NN}} = 62.4$ GeV are presented in Fig. 5.

Now the experimental ratios of $\bar{\Omega}^+$ to $\bar{\Lambda}$ remain larger than the QGSM predictions at high centralities, and, so, the new mechanism by which the three strange antiquarks needed for $\bar{\Omega}^+$ formation are taken from different Pomerons is still important, though its relative contribution decreases in comparison with CERN SpS energies.

On the other hand, the experimental ratios of $\bar{\Xi}^+$ to $\bar{\Lambda}$ are now in agreement with the QGSM model calculations, probably meaning that the production of $\bar{\Xi}^+$ inside one only Pomeron becomes more effective at this energy than the possibility of taking two strange antiquarks from different Pomerons.

This trend is confirmed by the STAR Collaboration data [50] at $\sqrt{s_{NN}} = 200$ GeV,

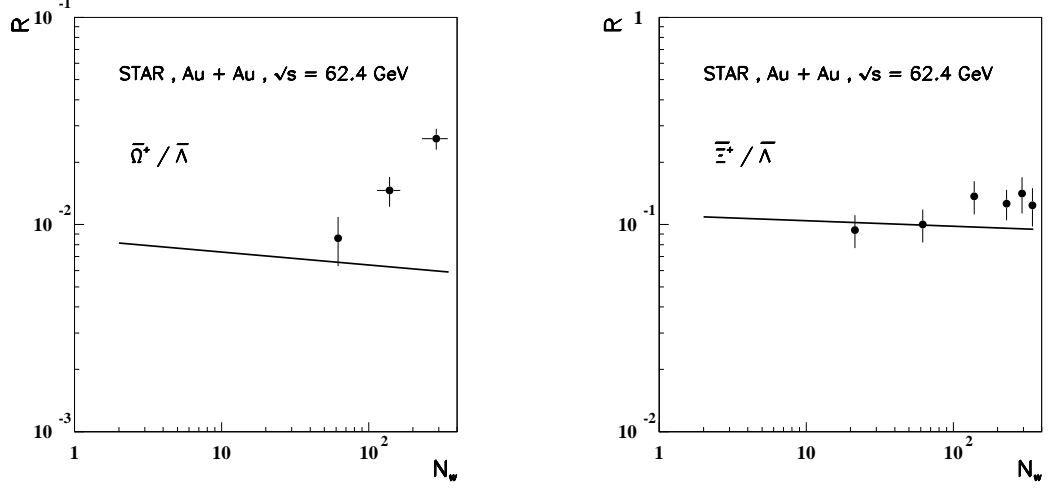


Figure 5: The experimental points obtained by the STAR Collaboration on the ratios of $\bar{\Omega}^+$ to $\bar{\Lambda}$ (left panel), and of $\bar{\Xi}^+$ to $\bar{\Lambda}$ (right panel), as functions of the number of wounded nucleons, N_w , for Au+Au collisions with different centralities, together with the corresponding QGSM results, shown by solid curves.

that are presented in Table 3 and in Fig. 6.

Collision	QGSM	STAR Collaboration
$\text{Cu}+\text{Cu} \rightarrow \bar{\Lambda}$	3.34	3.79 ± 0.37
$\text{Cu}+\text{Cu} \rightarrow \bar{\Xi}^+$	0.41	0.52 ± 0.8
$\text{Au}+\text{Au} \rightarrow \bar{\Lambda}$	13.3	14.7 ± 0.9
$\text{Au}+\text{Au} \rightarrow \bar{\Xi}^+$	1.66	—

Table 3: Experimental data [50] by the STAR Collaboration on $\bar{\Lambda}$ and $\bar{\Xi}^+$ production in central Cu+Cu and Au +Au collisions at $\sqrt{s_{NN}} = 200$ GeV, together with the corresponding QGSM results.

The ratios of $\bar{\Xi}^+$ to $\bar{\Lambda}$ at $\sqrt{s_{NN}} = 200$ GeV are in agreement with the QGSM calculations.

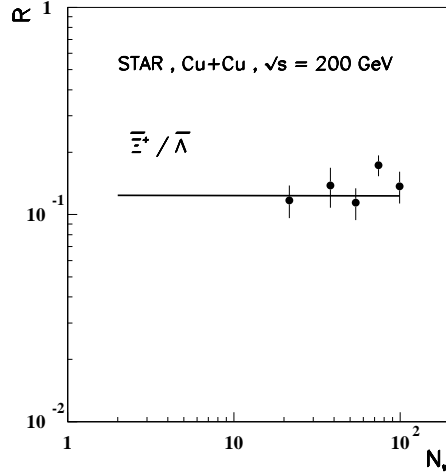


Figure 6: The experimental points obtained by the STAR Collaboration on the ratios of $\bar{\Xi}^+$ to $\bar{\Lambda}$ as functions of the number of wounded nucleons, N_w , for Au+Au collisions with different centralities, together with the corresponding QGSMM results, shown by solid curve.

5 Predictions for LHC and Conclusion

In nucleus-nucleus collisions, the number of quark-gluon strings (cut pomerons) increases with centrality. If the secondaries are independently produced in each quark-gluon string, the ratio of yields of different particles should not depend on centrality. However, it is experimentally clear (e.g. see [15], and Figs. 4 and 6) that the yield of $\bar{\Xi}^+$ is more strongly enhanced than that of $\bar{\Lambda}$, the same as the yield of $\Omega^- + \bar{\Omega}^+$ is more enhanced than that of Ξ^+ . This shows that an additional source of multistrange hyperons originated by the collective interactions of several strings must also play an active role, and then this additional source of multistrange hyperons can possibly be considered as a QGP signature.

If this scenario in which collective effects among different quark-gluon strings help in explaining the energy dependence from CERN SpS to RHIC of the production ratios of $\bar{\Omega}^+$ to $\bar{\Lambda}$ and of $\bar{\Xi}^+$ to $\bar{\Lambda}$, would be confirmed, one could not expect a significant dependence of these ratios on centrality (see Fig. 4 and left panel of Fig. 5), neither significant differences of these ratios at LHC energies from the QGSMM predictions, the expected values being $R(\bar{\Omega}^+/\bar{\Lambda}) \sim 0.14$ and $R(\bar{\Xi}^+/\bar{\Lambda}) \sim 0.014$.

A situation similar to the one shown in Figs. 4 can appear at LHC in Pb+Pb collisions in the midrapidity region for charmed antibaryon production, that is, for the

ratios $\overline{\Omega}_c^+ = \overline{c}ss$ to $\overline{\Lambda}_c$, and $\overline{\Xi}_c^+$ to $\overline{\Lambda}_c$.

In summary, we can assume that the considered Quark-Gluon Plasma formation events are rather rare, but at the same time they can be clearly identified by a well-defined selection trigger. At CERN SpS energy, such a trigger can be the $\overline{\Omega}^+$ production in central Au+Au collisions, where a strong centrality dependence of the ratio $\overline{\Omega}^+$ to $\overline{\Lambda}$ is apparent (see Fig. 4a).

Acknowledgements

We are grateful to C. Pajares for useful discussions and comments and to N.I. Novikova for technical help. This paper was supported by Ministerio de Economía y Competitividad of Spain (FPA2011–22776), the Spanish Consolider-Ingenio 2010 Programme CPAN (CSD2007-00042), by Xunta de Galicia, Spain (2011/PC043), by the State Committee of Science of the Republic of Armenia (Grant-13-1C023), and, partially, by grant RSGSS-3628.2008.2.

References

- [1] A.B. Kaidalov and K.A. Ter-Martirosyan, Yad. Fiz. **39**, 1545 (1984); **40**, 211 (1984).
- [2] A.B. Kaidalov and O.I. Piskounova, Yad. Fiz. **41**, 1278 (1985); Z. Phys. **C30**, 145 (1986).
- [3] Yu.M. Shabelski, Yad. Fiz. **44**, 186 (1986).
- [4] G.H. Arakelyan, C. Merino, C. Pajares, and Yu.M. Shabelski, Eur. Phys. J. **C54**, 577 (2008) and hep-ph/0709.3174.
- [5] C. Merino, C. Pajares and Yu.M. Shabelski, Eur. Phys. J. **C71**, 1652 (2011).
- [6] A.B. Kaidalov, K.A. Ter-Martirosyan, and Yu.M. Shabelski, Yad. Fiz. **43**, 1282 (1986).
- [7] Yu.M. Shabelski, Z. Phys. **C38**, 569 (1988).
- [8] Yu.M. Shabelski, Yad. Fiz. **50**, 239 (1989).
- [9] Yu.M. Shabelski, Z. Phys. **C57**, 409 (1993).
- [10] J. Dias de Deus and Yu.M. Shabelski, Yad. Fiz. **71**, 191 (2008).

- [11] G.H. Arakelyan, C. Merino, and Yu.M. Shabelski, arXiv:1305.0388 [hep-ph].
- [12] V.M. Braun and Yu.M. Shabelski, Int. J. Mod. Phys. **A3**, 2117 (1988).
- [13] G.D. Alkhazov *et al.*, Nucl. Phys. **A280**, 365 (1977).
- [14] A. Capella, A. Kaidalov, and J. Tran Thanh Van, Heavy Ion Phys. **9**, 169 (1999).
- [15] Huan Z. Huang, J. Phys. **G30**, 401 (2004).
- [16] V.A. Abramovsky, V.N. Gribov, and O.V. Kancheli, Yad. Fiz. **18**, 595 (1973).
- [17] A.B. Kaidalov, Sov. J. Nucl. Phys. **45**, 902 (1987); Yad. Fiz. **43**, 1282 (1986).
- [18] G.H. Arakelyan, A. Capella, A.B. Kaidalov, and Yu.M. Shabelski, Eur. Phys. J. C **26**, 81 (2002) and hep-ph/0103337.
- [19] Yu.M. Shabelski, Yad.Fiz. **26**, 1084 (1977); Nucl. Phys. **B132**, 491 (1978).
- [20] L. Bertocchi and D. Treleani, J. Phys. **G3**, 147 (1977).
- [21] J. Weis, Acta Phys. Polonica **B7**, 85 (1977).
- [22] T. Jaroszewicz *et al.*, Z. Phys. **C1**, 181 (1979).
- [23] B.B. Back *et al.* (PHOBOS Collaboration), Phys. Rev. Lett. **85**, 3100 (2000).
- [24] K. Adcox *et al.* (PHENIX Collaboration), Phys. Rev. Lett. **86**, 500 (2001).
- [25] A. Capella, C. Merino, and J. Tran Thanh Van, Phys. Lett. **B265** (1991) 415.
- [26] Yu.M. Shabelski, Z. Phys. **C57**, 409 (1993).
- [27] N. Armesto and C. Pajares, Int. J. Mod. Phys. **A15**, 2019 (2000).
- [28] O.V. Kancheli, JETP Lett. **18**, 274 (1973).
- [29] G.V. Davidenko and N.N. Nikolaev, Yad. Fiz. **24**, 772 (1976).
- [30] A. Schwimmer, Nucl. Phys. **B94**, 445 (1975).
- [31] J. Dias de Deus, R. Ugoccioni, and A. Rodrigues, Phys. Lett. **B458**, 402 (1999).
- [32] J. Dias de Deus, R. Ugoccioni, and A. Rodrigues, Eur. Phys. J. **C16**, 537 (2000).
- [33] M.A. Braun and C. Pajares, Phys. Rev. Lett. **85**, 4864 (2000).

- [34] J. Dias de Deus and Yu.M. Shabelski, Eur. Phys. J. **A20**, 457 (2004).
- [35] P. Brogueira, J. Dias de Deus, and C. Pajares, Phys. Rev. **C75**, 054908 (2007).
- [36] C. Merino, C. Pajares, and J. Ranft, Phys. Lett. **B276**, 168 (1992).
- [37] H.J. Möhring, J. Ranft, C. Merino, and C. Pajares, Phys. Rev. **D47**, 4142 (1993).
- [38] N.S. Amelin, M.A. Braun, and C. Pajares, Z. Phys. **C63**, 507 (1994).
- [39] I. Bautista, C. Pajares, and J. Dias de Deus, Nucl. Phys. **A882**, 44 (2012).
- [40] I. Bautista, J. Dias de Deus, G. Milhano, and C. Pajares, Phys. Lett. **B715**, 230 (2012).
- [41] I. Bautista, C. Pajares, G. Milhano, and J. Dias de Deus, Phys. Rev. **C86**, 034909 (2012).
- [42] M.A. Braun and C. Pajares, Eur. Phys. J. **C16**, 2019 (2000).
- [43] C. Merino, C. Pajares, and Yu.M. Shabelski, Eur. Phys. J. **C59**, 691 (2009) and arXiv:0802.2195[hep-ph].
- [44] J. Dias de Deus and C. Pajares, Phys. Lett. **B695**, 211 (2012) and arXiv:1011.1099[hep-ph].
- [45] A.V. Efremov *et al.*, Phys. Atom. Nucl. **57**, 874 (1994).
- [46] T. Anticic *et al.* (NA44 Collaboration), Phys. Rev. **C80**, 034906 (2009) and arXiv:0906.0469[nucl-ex].
- [47] T. Anticic *et al.* (NA44 Collaboration), Phys. Rev. **C78**, 034918 (2008) and arXiv:0804.3770[nucl-ex].
- [48] F. Antinori *et al.* (NA57 Collaboration), J. Phys. **G32**, 427 (2006) and arXiv:0601021[nucl-ex].
- [49] M.M. Aggarwal *et al.* (STAR Collaboration), Phys. Rev. **C83**, 024901 (2011) and arXiv:1010.0146[nucl-ex].
- [50] G. Agakishiev *et al.* (STAR Collaboration), Phys. Rev. Lett. **108**, 072301 (2012) and arXiv:1107.2955[nucl-ex].